ACS OMEGA

http://pubs.acs.org/journal/acsodf

Article

First-Principles Study of Structural and Electronic Properties of Monolayer PtX_2 and Janus PtXY (X, Y = S, Se, and Te) via Strain Engineering

Xun Ge, Xiaohao Zhou,* Deyan Sun,* and Xiaoshuang Chen

Cite This: *ACS Omega* 2023, 8, 5715−5721

Read Online

ACCESS | Metrics & More | Article Recommendations

ABSTRACT: In this work, the structural parameters and electronic properties of PtX_2 and Janus PtXY (X, Y = S, Se, and Te) are studied based on the density functional theory. The phonon spectra and the Born criteria of the elastic constant of these six monolayers confirm their stability. All PtX_2 and Janus PtXY monolayers show an outstanding stretchability with Young's modulus ranging from 61.023 to 82.124 N/m, about one-fifth that of graphene and half that of MoS_2, suggesting highly flexible materials. Our first-principles calculations reveal that the pristine PtX_2 and their Janus counterparts are indirect semiconductors with their band gap ranging from 0.760 to 1.810 eV at the Perdew−Burke−Ernzerhof level (1.128−2.580 eV at the Heyd−Scuseria−Ernzerhof level). By applying biaxial compressive and tensile strain, the electronic properties of all PtX_2 and Janus PtXY monolayers are widely tunable. Under small compressive strain, PtX_2 and Janus PtXY structures remain indirect semiconductors. $PtTe_2$, PtSeTe, and PtSTe monolayers undergo a semiconducting to metallic transition when the strain reaches −6, −8, and −10%, respectively. Interestingly, there is a transition from the indirect semiconductor to a quasi-direct one for all PtX_2 and Janus PtXY monolayers when the tensile strain is applied.

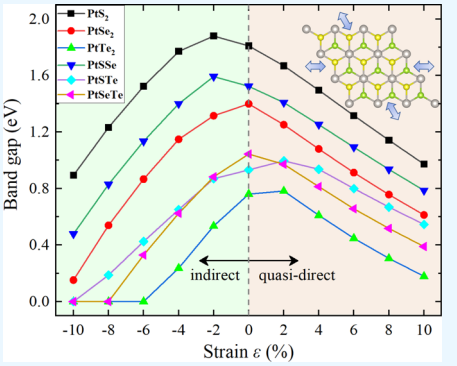

INTRODUCTION

Two-dimensional materials have attracted enormous attentions and provided an exciting platform for great potential applications in optoelectronics, electronics, spintronics, and Li-ion batteries, owing to the fascinating properties.[1−5] Among them, 2D transitional metal dichalcogenides (TMDs) with the general chemical formula MX_2, where one transition metal (M) sublayer is sandwiched between two sublayers of chalcogenide (X) atoms, exhibit exceptional properties such as superior environmental stability, flexibility, high carrier mobility, and layer-dependent band structure tunability.[6−10] Initially, the research hot spots of TMDs are mainly concentrated on the group VI B transition metals (M = Mo and W). Recently, the noble metal dichalcogenides (such as PtS_2, $PtSe_2$, $PtTe_2$, PdS_2, etc.) have emerged as promising candidates for potential novel applications in mid-infrared photonics, optoelectronics, electronics, and photocatalysis, owing to their exceptional properties. A novel $PtSe_2$ monolayer is successfully fabricated and found to be semiconducting compared to its semi-metallic bulk phase.[11] The band gaps of monolayer and bilayer $PtSe_2$ are widely tuned via strain engineering by the first-principles calculations.[12] Few-layer PtS_2 is experimentally investigated to present a layer-dependent indirect band gap and high mobility.[13] PtS_2 and $PtSe_2$ are theoretically predicted to have a high carrier mobility (larger than 1000 $cm^2\ V^{-1}\ s^{-1}$) at room temperature.[14]

One of the most special structures that were first fabricated in the experiment[15] is the so-called Janus material, a 2D material with planar asymmetry. The Janus structures are formed with one layer of X in MX_2 replaced by another chalcogen Y layer, owning a general formula of MXY. They possess distinct properties that are distinguished from those of pristine MX_2 due to the breaking of the mirror symmetry. Compared with pristine $MoSe_2$, Janus MoSSe endows it with intrinsic polarity, enabling richer properties. Janus materials have received increasing attention with their distinct physical properties that are different from those of conventional 2D materials.[16−19] The creation of asymmetric materials from existing symmetric ones has provided a new way to tune the electronic properties of 2D materials. Since the successful fabrication of MoSSe, more and more attention has been paid to other Janus materials, such as MoXY,[20,21] WXY,[22−24] PtXY,[25,26] HfXY,[27,28] and SnXY[29,30] (X, Y = S, Se, and Te). The photocatalytic properties of monolayer and bilayer PtSSe are revealed to be superior to those of PtS_2 and $PtSe_2$.[25]

Received: November 12, 2022
Accepted: January 25, 2023
Published: February 3, 2023

https://doi.org/10.1021/acsomega.2c07271
ACS Omega 2023, 8, 5715−5721

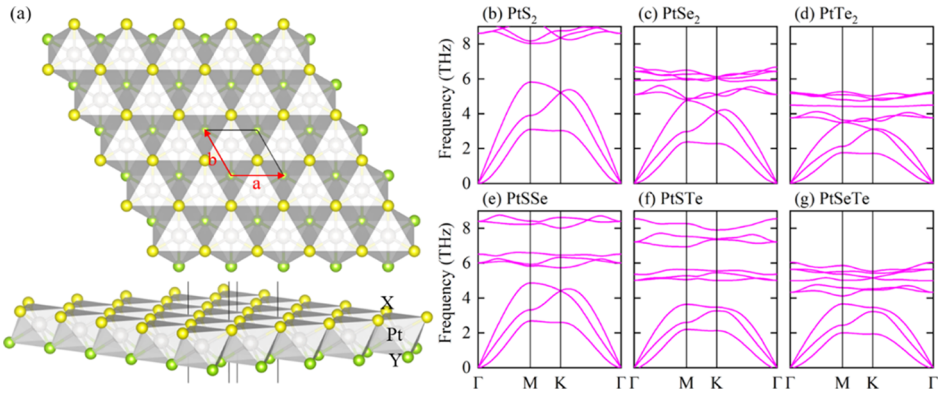

Figure 1. (a) Top and side views of the Janus PtXY monolayer where gray balls represent Pt atoms and yellow and green ones indicate chalcogen atoms. Phonon dispersions of pristine (b–d) PtX_2 and (e–g) Janus PtXY (X, Y = S, Se, and Te), respectively.

Table 1. Calculated Lattice Constant *a*, Bond Lengths *d*, Band Gap at the PBE and HSE06 Levels, Elastic Constants C_{ij}, Young's Modulus $Y(\theta)$, and Poisson's Ratio $\nu(\theta)$ of the Optimized PtX_2 and Janus PtXY Monolayers

	a (Å)	$d_{Pt\text{-}X}$ (Å)	$d_{Pt\text{-}Y}$ (Å)	E_g^{PBE} (eV)	E_g^{HSE06} (eV)	C_{11}(N/m)	C_{12}(N/m)	C_{66}(N/m)	$Y(\theta)$ (N/m)	$\nu(\theta)$
PtS_2	3.571	2.399		1.810	2.580	88.488	23.731	32.379	82.124	0.268
$PtSe_2$	3.748	2.528		1.399	1.935	72.880	19.728	26.576	67.540	0.271
$PtTe_2$	4.018	2.705		0.760	1.128	66.146	18.153	23.997	61.164	0.274
PtSSe	3.659	2.430	2.500	1.523	2.208	78.248	20.586	28.831	72.832	0.263
PtSTe	3.809	2.498	2.625	0.931	1.489	65.616	17.360	24.128	61.023	0.265
PtSeTe	3.892	2.591	2.650	1.044	1.508	65.889	17.800	24.044	61.080	0.270

Different combinations of PtX_2 and Janus PtXY can form type-I, type-II, and type-III heterojunctions, respectively.[31] The strength of the Rashba effect and the band gap of Janus PtXY under strain are investigated to demonstrate the potential application for spintronics.[32] The absorption intensity and peak as well as electronic properties of monolayer PtSSe are significantly modified via the electric field and strain.[33] Very recently, it was reported that the PtSSe monolayer is sensitive to tensile strains, while the PtSTe and PtSeTe monolayers are compressive strain-sensitive.[34] Although a multitude of research studies have been reported, there is a lack of detailed comparison of mechanical properties and electronic properties under the biaxial strain between pristine PtX_2 and Janus PtXY.

In this work, we systematically investigate the structural, mechanical, and electronic properties of Janus PtXY (X, Y = S, Se, and Te) monolayers compared with those of their parent structures by means of the density functional theory. It shows that all these studied monolayers are dynamically stable and stretchable, which can be synthesized as free-standing materials. They are calculated to be indirect band gap semiconductors and lattice constants as well as band gaps of the Janus PtXY monolayers fall in between those of their parent compounds. The strain-dependent electronic properties of these materials are also systematically investigated. These six monolayers remain indirect semiconductors under small compressive strain but turn out to be quasi-direct semiconductors when the tensile strain is applied.

CALCULATION DETAILS

Our calculations are performed using the Vienna ab initio simulation package (VASP)[35,36] with the projector augmented wave[37] method. The generalized gradient approximation of the Perdew–Burke–Ernzerhof (PBE)[38] functional is chosen to address the exchange–correlation energy. Through the calculations, the plane-wave cutoff energy is set to 450 eV. The criteria of energy convergence and forces on each atom are set to 10^{-5} eV and 0.01 eV/Å, respectively. The *k*-mesh of 12 × 12 × 1 is used to sample the first Brillouin zone of pure PtX_2 and Janus PtXY. In order to avoid interactions between neighboring images, a vacuum layer thickness of 15 Å in the vertical direction is added. The phonon calculations are carried out using the PHONOPY code.[39] In addition, as the PBE functional generally underestimates the band gap of semiconductors, the Heyd–Scuseria–Ernzerhof (HSE06)[40] functional is also considered to correct the band diagrams. The charge transfer in the structures is determined by the Bader charge analysis.[41]

In terms of the mechanical properties, the Young's modulus $Y(\theta)$ and Poisson's ratio $\nu(\theta)$ along the in-plane θ (the polar angle relative to the a-axis) can be expressed as[42]

$$Y(\theta) = \frac{C_{11}C_{22} - C_{12}^2}{C_{22}\cos^4\theta + A\sin^2\theta\cos^2\theta + C_{11}\sin^4\theta} \quad (1)$$

$$\nu(\theta) = \frac{C_{12}\cos^4\theta - B\sin^2\theta\cos^2\theta + C_{12}\sin^4\theta}{C_{22}\cos^4\theta + A\sin^2\theta\cos^2\theta + C_{11}\sin^4\theta} \quad (2)$$

where C_{ij} represents the elastic constants, $A = (C_{11}C_{22} - C_{12}^2)/C_{66} - 2C_{12}$ and $B = C_{11} + C_{22} - (C_{11}C_{22} - C_{12}^2)/C_{66}$.

RESULTS AND DISCUSSION

Unlike most TMD semiconductors owning a 2H stable phase, the 1T phase of pristine PtX_2 is thermodynamically favored.[43,44] Janus PtXY structures are obtained by replacing one side X atoms of PtX_2 by another Y chalcogen atoms, as shown in Figure 1a. The unit cell contains one Pt atom and

https://doi.org/10.1021/acsomega.2c07271
ACS Omega 2023, 8, 5715–5721

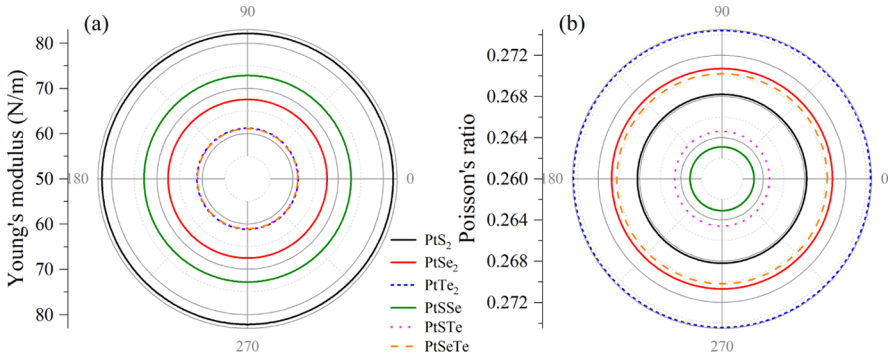

Figure 2. Calculated (a) Young's modulus and (b) Poisson's ratio of pristine PtX_2 and Janus PtXY monolayers as a function of the in-plane angle θ.

two chalcogen atoms, where the stacking sequence of atomic layers is X−Pt−Y. The calculated structural parameters of PtX_2 and Janus PtXY monolayers are summarized in Table 1. The lattice constants a are 3.571, 3.748, 4.018, 3.659, 3.809, and 3.892 Å for PtS_2, $PtSe_2$, $PtTe_2$, PtSSe, PtSTe, and PtSeTe monolayers, respectively, which increase with the increasing atomic number of group VI A elements (X or Y). The bond lengths $d_{Pt\text{-}X}$ or $d_{Pt\text{-}Y}$ also have the same trend. For instance, the PtSSe monolayer shows the smallest a and $d_{Pt\text{-}X}$ (or $d_{Pt\text{-}Y}$), while PtSeTe exhibits the largest ones among PtXY configurations. To confirm the dynamical stability of pristine PtX_2 and Janus PtXY, we calculate their phonon frequency spectra. As shown in Figure 1b−g, there are no imaginary modes in the whole Brillouin zone, revealing the dynamical stability of all these structures.

Moreover, we examine the mechanical properties of monolayer PtX_2 and Janus PtXY through the analysis of their elastic constants C_{ij}. The calculated C_{ij} constants of PtX_2 and Janus PtXY are listed in Table 1. Since C_{22} is equal to C_{11}, we are able to draw the conclusion that all PtX_2 and Janus PtXY monolayers are mechanically stable under small deformations upon satisfying the Born criteria:[45] $C_{11}C_{22} > C_{12}^2$ and $C_{66} > 0$. Next, we can get the Young's modulus $Y(\theta)$ and Poisson's ratio $\nu(\theta)$ of PtX_2 and Janus PtXY based on the calculated C_{ij} elastic constants.[42] From Figure 2, it can be seen that the Young's modulus and Poisson's ratio of all six materials do not change with respect to the in-plane θ, exhibiting strong isotropy. It is calculated that $Y(\theta)$ values of monolayer PtS_2, $PtSe_2$, $PtTe_2$, PtSSe, PtSTe, and PtSeTe are 82.124, 67.540, 61.164, 72.832, 61.023, and 61.080 N/m, respectively. It seems that the presence of a larger chalcogenide atom contributes to a more flexible material. Nevertheless, the values of PtSTe and PtSeTe are almost the same, so they nearly overlap with that of $PtTe_2$ in Figure 2a. Compared with some common two-dimensional materials, pure PtX_2 and Janus PtXY studied here are less rigid, with $Y(\theta)$ values one-fifth that of graphene[46] and one-half that of MoS_2.[10,47] In addition, $\nu(\theta)$ values of PtS_2, $PtSe_2$, $PtTe_2$, PtSSe, PtSTe, and PtSeTe are 0.268, 0.271, 0.274, 0.263, 0.265, and 0.270, respectively. The above results suggest that PtX_2 and Janus PtXY monolayers are highly stretchable and may have potential applications in flexible electronics and wearable electronic devices. From phonon dispersion and elastic constants, it is shown that all PtX_2 and Janus PtXY monolayers are dynamically and mechanically stable.

Based on the optimized structures, the electronic band structures of PtX_2 and Janus PtXY monolayers are plotted in Figure 3, all exhibiting a semiconducting property with an indirect band gap. The locations of the conduction band

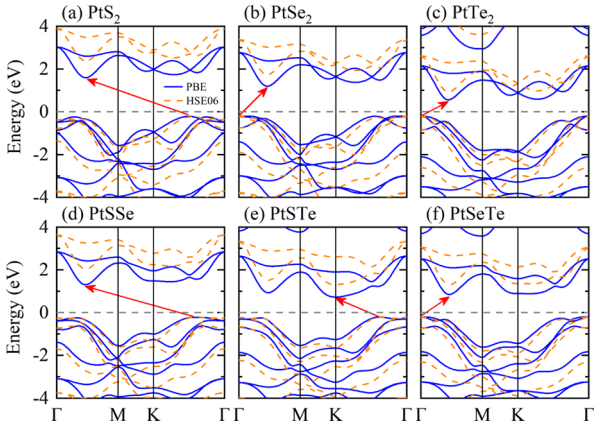

Figure 3. Energy bands of (a−c) PtX_2 and (d−f) Janus PtXY monolayers at the PBE (blue solid lines) and HSE06 (orange dashed lines) functionals. The Fermi level is set to 0 eV.

minimum (CBM) of all PtX_2 and Janus PtXY configurations turn out to be along the Γ−M direction except for the CBM of PtSTe at the K point. The sites of the valence band maximum (VBM) of PtS_2, PtSSe, and PtSTe are on the Γ−K path, while those of $PtSe_2$, $PtTe_2$, and PtSeTe are at the Γ point. The band gaps of PtX_2 and Janus PtXY follow the order PtS_2 > PtSSe > $PtSe_2$ > PtSeTe > PtSTe > $PtTe_2$, with the values of 1.810, 1.523, 1.399, 1.044, 0.931, and 0.760 eV at the PBE level, respectively. PtS_2 monolayer owns the largest band gap, whereas $PtTe_2$ possesses the smallest one among all six monolayers. The gap of Janus PtXY is between the values of pristine PtX_2 and PtY_2. Our results are in good agreement with previous studies.[11,13,32] The band gap calculated by the PBE functional is well known to underestimate the actual energy gap of semiconductors. To compensate for this influence, the HSE06 functional is also taken into account to obtain more accurate electronic properties. The resulting bands at the HSE06 level inherit the overall shape of those determined by the PBE functional, with the band gaps increasing to 2.580, 2.208, 1.935, 1.508, 1.489, and 1.128 eV for PtS_2, PtSSe, $PtSe_2$, PtSeTe, PtSTe, and $PtTe_2$ monolayers, respectively, due to the shifting of the conduction bands to the higher energy levels.

Strain engineering is one of the most common and effective ways to achieve tunable electronic properties of 2D materials.[48−52] Here, we examine the influence of a biaxial strain on the electronic structures of PtX_2 and Janus PtXY. The biaxial strain ε is defined by $\varepsilon = (a - a_0)/a_0$, where a and a_0 are the lattice constants of PtX_2/PtXY with and without strain, respectively. In the current calculations, a biaxial strain ranging

https://doi.org/10.1021/acsomega.2c07271
ACS Omega 2023, 8, 5715−5721

from −10 and 10% is applied. The minus (plus) sign denotes the compressive (tensile) strain.

The band structures of PtX_2 and Janus PtXY under the biaxial tensile strains are shown in Figure 4. It reveals that the

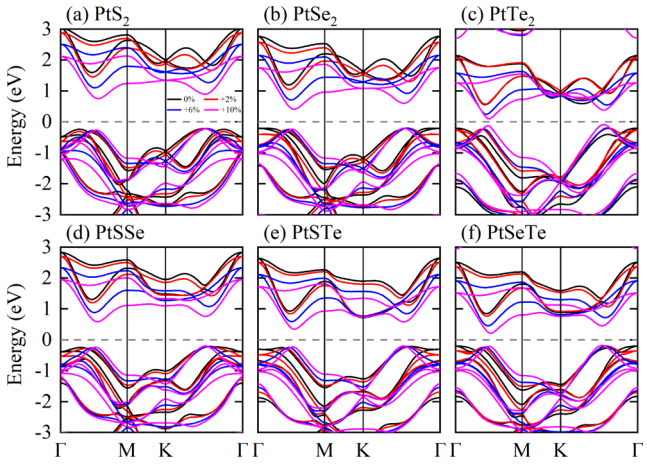

Figure 4. Calculated PBE band structures of (a) PtS_2, (b) $PtSe_2$, (c) $PtTe_2$, (d) PtSSe, (e) PtSTe, and (f) PtSeTe under biaxial tensile strains. The dashed gray lines indicate the Fermi level.

electronic structures of PtX_2 and Janus PtXY are significantly modified by the biaxial strain ε. When 2% tensile strain is applied, the CBM positions of all PtX_2 and Janus PtXY configurations remain on the Γ−*M* path excluding PtSTe. With the increase of tensile strain (greater than 2%), the lowest unoccupied band of PtSTe along the Γ−*M* path drops lower than that at the K point, leading to the formation of a new CBM, as shown in Figure 4e. The VBM sites of $PtSe_2$, $PtTe_2$, and PtSeTe monolayers have moved to the Γ−*K* path instead of the Γ point under the tensile strain. Due to the existence of the sub-VBM on the Γ−*M* path, which is quite close to the true VBM along the Γ−*K* path, all PtX_2 and PtXY can also be considered as a quasi-direct band gap semiconductor under the tensile strain.

As the compressive strain is applied, the CBM of PtSTe remains at the K point until it crosses the Fermi level when strain ε reaches −10%, as given in Figure 5e. However, for other monolayers investigated here, there is a competition in the lowest unoccupied band around the Brillouin zone,

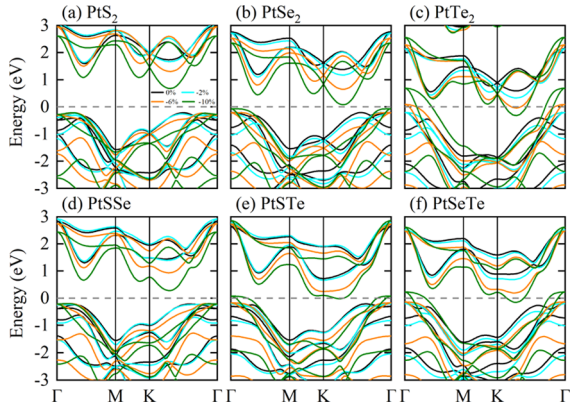

Figure 5. Calculated PBE band structures of (a) PtS_2, (b) $PtSe_2$, (c) $PtTe_2$, (d) PtSSe, (e) PtSTe, and (f) PtSeTe under biaxial compressive strains. The dashed gray lines indicate the Fermi level.

meaning that the CBM has changed from the Γ−*M* direction (pristine structures) to the Γ−*K* direction. Under the small compressive strain, PtX_2 and Janus PtXY monolayers are still indirect semiconductors with the decrease of the band gap. With the further increase in ε, $PtTe_2$, PtSeTe, and PtSTe monolayers turn out to be metallic when biaxial strain ε reaches −6, −8, and −10%, respectively.

From Figures 4 and 5, it can be seen that the valence bands of PtX_2 and PtXY are more sensitive to the compressive strain; however, the conduction bands are more sensitive to the tensile strain. To clearly illustrate the variation trend of electronic properties under the biaxial strain, we take the PtSSe monolayer as an example. The projected band structures of PtSSe under different biaxial strains are plotted in Figure 6. The VBM of PtSSe is mainly dominated by the p orbitals from S and Se atoms, while the main contribution to the CBM originates from the d orbital of the Pt atom and the contribution from S-p and Se-p orbitals is relatively small. When the compressive strain is applied, the site of the CBM is unchanged and the highest occupied band at the Γ point drops faster than that at other *k*-points with two obvious peaks occurring around the Brillouin zone. The sub-VBM on the Γ−*M* path is nearly the same as the true VBM along the Γ−*K* path. Therefore, PtSSe can be regarded as a quasi-direct band gap semiconductor under the tensile strain. When the −2% compressive strain is added, the locations of the CBM and VBM remain unchanged compared to that in the pristine structure. With the increase in the tensile strain, a new CBM appears along the Γ−*K* path instead of the Γ−*M* path and the band gap decreases as well.

According to the Bader analysis in Figure 7, the charge transferring from central Pt atoms to outer S and Se atoms are about 0.22 e and 1.68×10^{-3} e, respectively, when the PtSSe monolayer is free of strain. In terms of the overall trend, the charge mainly transfers from Pt atoms to S atoms when the biaxial (tensile or compressive) strain is applied. As the tensile strain is increased to +6%, the charge from Se atoms decreases by about 0.02 e. However, Se atoms get 0.05 e charge as the compressive strain is increased to −6%.

From the results above, it is observed that the movement of the band edge and gaps are highly sensitive to the applied strain. The quantitative relationship between the strain and the band gap of PtX_2 and Janus PtXY is summarized in Figure 8. It can be seen that electronic properties of PtX_2 and Janus PtXY can be widely regulated by the biaxial strain and the band gaps of Janus PtXY distribute between those of pristine PtX_2 and PtY_2. With the increase of tensile strain, the gap decreases in an almost linear manner excluding $PtTe_2$ and PtSTe. Band gaps of $PtTe_2$ and PtSTe increase to 0.780 and 0.995 eV when the strain is 2%, respectively, and then decrease with the further increase in strain. It can lead to the conclusion that phonon energy used for electronic excitation is reduced when the structures are subject to the tensile strain owing to their quasi-direct bands. Under a −2% compressive strain, the gaps of PtS_2 and PtSSe reach the maximum values of 1.880 and 1.593 eV, respectively, and then decrease gradually with the increase of ε. The gaps of other PtXY and PtX_2 decrease monotonically as a function of compressive strain ε until those of $PtTe_2$, PtSeTe, and PtSTe disappear at the −6, −8, and −10% strains, respectively.

https://doi.org/10.1021/acsomega.2c07271
ACS Omega 2023, 8, 5715−5721

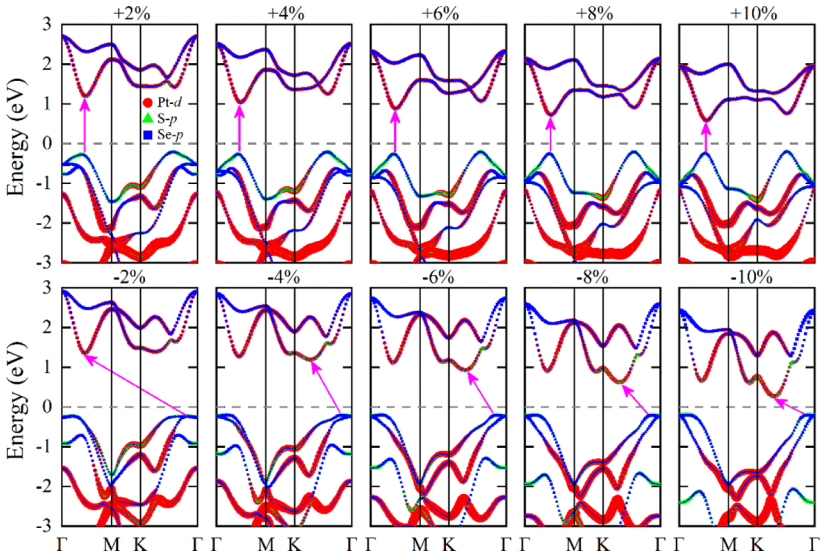

Figure 6. Projected band structures of PtSSe under different tensile and compressive strains. The symbols of red circle, green triangle, and blue square denote the contributions from Pt-d and S-/Se-p orbitals, respectively.

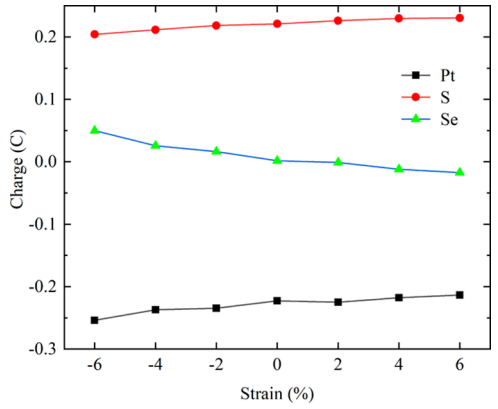

Figure 7. Bader charge for the PtSSe monolayer as a function of biaxial strains.

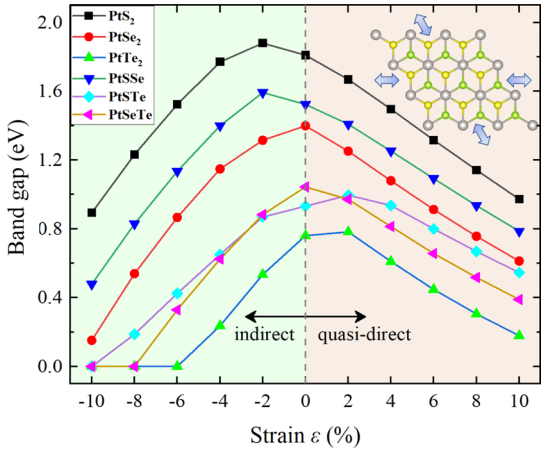

Figure 8. Variation of the band gap of PtX_2 and Janus PtXY monolayers with the applied biaxial strain under the PBE functional.

CONCLUSIONS

In summary, we have considered the structural, stability, and electronic properties of PtX_2 and Janus PtXY monolayers characterized by first-principles calculations. PtX_2 and Janus PtXY structures are found to be dynamically and mechanically stable and less rigid than common 2D materials, which can be applied in wearable devices. At the ground state, all PtX_2 and Janus PtXY monolayers are indirect semiconductors with the gap ranging from 0.760 to 1.810 eV at the PBE functional. What is more, the electronic properties of these monolayers can be widely tuned by the biaxial strain. When small compressive strain is applied, all monolayers exhibit an indirect band gap with the decrease of values. $PtTe_2$, PtSeTe, and PtSTe structures become metallic when ε reaches −6, −8, and −10%, respectively. However, all PtX_2 and PtXY can undergo a transition from an indirect band gap to a quasi-direct band gap with the increase of tensile strain, facilitating the efficiency of photoelectric coupling. Therefore, our results provide a promising platform for nanoelectronics and optoelectronics.

AUTHOR INFORMATION

Corresponding Authors

Xiaohao Zhou − *State Key Laboratory of Infrared Physics, Shanghai Institute of Technical Physics, Chinese Academy of Sciences, Shanghai 200083, China*; Email: xhzhou@mail.sitp.ac.cn

Deyan Sun − *Engineering Research Center for Nanophotonics & Advanced Instrument (MOE), School of Physics and Electronic Science, East China Normal University, Shanghai 200241, China*; orcid.org/0000-0002-9728-8017; Email: dysun@phy.ecnu.edu.cn

Authors

Xun Ge − *Engineering Research Center for Nanophotonics & Advanced Instrument (MOE), School of Physics and Electronic Science, East China Normal University, Shanghai 200241, China; State Key Laboratory of Infrared Physics, Shanghai Institute of Technical Physics, Chinese Academy of Sciences, Shanghai 200083, China*; orcid.org/0000-0002-2668-408X

Xiaoshuang Chen − *State Key Laboratory of Infrared Physics, Shanghai Institute of Technical Physics, Chinese Academy of Sciences, Shanghai 200083, China*

Complete contact information is available at:

https://doi.org/10.1021/acsomega.2c07271
ACS Omega 2023, 8, 5715−5721

https://pubs.acs.org/10.1021/acsomega.2c07271

Notes

The authors declare no competing financial interest.

■ ACKNOWLEDGMENTS

The project was supported by the National Natural Science Foundation of China (grant no. 12274127) and by the National Key Research and Development Program of China (grant no. 2022YFA1404603). The computations were supported by National SuperComputer Center in Tianjin.

■ REFERENCES

(1) Chaves, A.; Azadani, J. G.; Alsalman, H.; da Costa, D. R.; Frisenda, R.; Chaves, A. J.; Song, S. H.; Kim, Y. D.; He, D.; Zhou, J.; Castellanos-Gomez, A.; Peeters, F. M.; Liu, Z.; Hinkle, C. L.; Oh, S.-H.; Ye, P. D.; Koester, S. J.; Lee, Y. H.; Avouris, P.; Wang, X.; Low, T. Bandgap engineering of two-dimensional semiconductor materials. *npj 2D Mater. Appl.* **2020**, *4*, 29.

(2) Mak, K. F.; Shan, J.; Ralph, D. C. Probing and controlling magnetic states in 2D layered magnetic materials. *Nat. Rev. Phys.* **2019**, *1*, 646−661.

(3) Wang, Q. H.; Kalantar-Zadeh, K.; Kis, A.; Coleman, J. N.; Strano, M. S. Electronics and optoelectronics of two-dimensional transition metal dichalcogenides. *Nat. Nanotechnol.* **2012**, *7*, 699−712.

(4) Castro Neto, A. H.; Guinea, F.; Peres, N. M. R.; Novoselov, K. S.; Geim, A. K. The electronic properties of graphene. *Rev. Mod. Phys.* **2009**, *81*, 109−162.

(5) Anasori, B.; Lukatskaya, M. R.; Gogotsi, Y. 2D metal carbides and nitrides (MXenes) for energy storage. *Nat. Rev. Mater.* **2017**, *2*, 16098.

(6) Ciarrocchi, A.; Avsar, A.; Ovchinnikov, D.; Kis, A. Thickness-modulated metal-to-semiconductor transformation in a transition metal dichalcogenide. *Nat. Commun.* **2018**, *9*, 919.

(7) Kuc, A.; Zibouche, N.; Heine, T. Influence of quantum confinement on the electronic structure of the transition metal sulfide TS_2. *Phys. Rev. B: Condens. Matter Mater. Phys.* **2011**, *83*, 245213.

(8) Mak, K. F.; Lee, C.; Hone, J.; Shan, J.; Heinz, T. F. Atomically Thin MoS_2: A New Direct-Gap Semiconductor. *Phys. Rev. Lett.* **2010**, *105*, 136805.

(9) Wang, Z.; Li, Q.; Besenbacher, F.; Dong, M. Facile Synthesis of Single Crystal $PtSe_2$ Nanosheets for Nanoscale Electronics. *Adv. Mater.* **2016**, *28*, 10224−10229.

(10) Liu, K.; Yan, Q.; Chen, M.; Fan, W.; Sun, Y.; Suh, J.; Fu, D.; Lee, S.; Zhou, J.; Tongay, S.; Ji, J.; Neaton, J. B.; Wu, J. Elastic Properties of Chemical-Vapor-Deposited Monolayer MoS_2, WS_2, and Their Bilayer Heterostructures. *Nano Lett.* **2014**, *14*, 5097−5103.

(11) Wang, Y.; Li, L.; Yao, W.; Song, S.; Sun, J. T.; Pan, J.; Ren, X.; Li, C.; Okunishi, E.; Wang, Y.-Q.; Wang, E.; Shao, Y.; Zhang, Y. Y.; Yang, H.-t.; Schwier, E. F.; Iwasawa, H.; Shimada, K.; Taniguchi, M.; Cheng, Z.; Zhou, S.; Du, S.; Pennycook, S. J.; Pantelides, S. T.; Gao, H.-J. Monolayer $PtSe_2$, a New Semiconducting Transition-Metal-Dichalcogenide, Epitaxially Grown by Direct Selenization of Pt. *Nano Lett.* **2015**, *15*, 4013−4018.

(12) Li, P.; Li, L.; Zeng, X. C. Tuning the electronic properties of monolayer and bilayer $PtSe_2$ via strain engineering. *J. Mater. Chem. C* **2016**, *4*, 3106−3112.

(13) Zhao, Y.; Qiao, J.; Yu, P.; Hu, Z.; Lin, Z.; Lau, S. P.; Liu, Z.; Ji, W.; Chai, Y. Extraordinarily Strong Interlayer Interaction in 2D Layered PtS_2. *Adv. Mater.* **2016**, *28*, 2399−2407.

(14) Zhang, W.; Huang, Z.; Zhang, W.; Li, Y. Two-dimensional semiconductors with possible high room temperature mobility. *Nano Res.* **2014**, *7*, 1731−1737.

(15) Lu, A.-Y.; Zhu, H.; Xiao, J.; Chuu, C.-P.; Han, Y.; Chiu, M.-H.; Cheng, C.-C.; Yang, C.-W.; Wei, K.-H.; Yang, Y.; Wang, Y.; Sokaras, D.; Nordlund, D.; Yang, P.; Muller, D. A.; Chou, M.-Y.; Zhang, X.; Li, L.-J. Janus monolayers of transition metal dichalcogenides. *Nat. Nanotechnol.* **2017**, *12*, 744−749.

(16) Dong, L.; Lou, J.; Shenoy, V. B. Large In-Plane and Vertical Piezoelectricity in Janus Transition Metal Dichalchogenides. *ACS Nano* **2017**, *11*, 8242−8248.

(17) Riis-Jensen, A. C.; Pandey, M.; Thygesen, K. S. Efficient Charge Separation in 2D Janus van der Waals Structures with Built-in Electric Fields and Intrinsic p-n Doping. *J. Phys. Chem. C* **2018**, *122*, 24520−24526.

(18) Palsgaard, M.; Gunst, T.; Markussen, T.; Thygesen, K. S.; Brandbyge, M. Stacked Janus Device Concepts: Abrupt pn-Junctions and Cross-Plane Channels. *Nano Lett.* **2018**, *18*, 7275−7281.

(19) Wang, J.; Zhang, D.; Zhou, B. Achieving an Ohmic contact in graphene-based van der Waals heterostructures by intrinsic defects and the inner polarized electric field of Janus AlGaSSe. *New J. Chem.* **2021**, *45*, 21178−21187.

(20) Yagmurcukardes, M.; Sevik, C.; Peeters, F. M. Electronic, vibrational, elastic, and piezoelectric properties of monolayer Janus MoSTe phases: A first-principles study. *Phys. Rev. B* **2019**, *100*, 045415.

(21) Wang, J.; Shu, H.; Zhao, T.; Liang, P.; Wang, N.; Cao, D.; Chen, X. Intriguing electronic and optical properties of two-dimensional Janus transition metal dichalcogenides. *Phys. Chem. Chem. Phys.* **2018**, *20*, 18571−18578.

(22) Er, D.; Ye, H.; Frey, N. C.; Kumar, H.; Lou, J.; Shenoy, V. B. Prediction of Enhanced Catalytic Activity for Hydrogen Evolution Reaction in Janus Transition Metal Dichalcogenides. *Nano Lett.* **2018**, *18*, 3943−3949.

(23) Zhou, W.; Chen, J.; Yang, Z.; Liu, J.; Ouyang, F. Geometry and electronic structure of monolayer, bilayer, and multilayer Janus WSSe. *Phys. Rev. B* **2019**, *99*, 075160.

(24) Ju, L.; Bie, M.; Tang, X.; Shang, J.; Kou, L. Janus WSSe Monolayer: An Excellent Photocatalyst for Overall Water Splitting. *ACS Appl. Mater. Interfaces* **2020**, *12*, 29335−29343.

(25) Peng, R.; Ma, Y.; Huang, B.; Dai, Y. Two-dimensional Janus PtSSe for photocatalytic water splitting under the visible or infrared light. *J. Mater. Chem. A* **2019**, *7*, 603−610.

(26) Cao, L.; Ang, Y. S.; Wu, Q.; Ang, L. K. Janus PtSSe and graphene heterostructure with tunable Schottky barrier. *Appl. Phys. Lett.* **2019**, *115*, 241601.

(27) Dimple, D.; Jena, N.; Rawat, A.; Ahammed, R.; Mohanta, M. K.; De Sarkar, A. Emergence of high piezoelectricity along with robust electron mobility in Janus structures in semiconducting Group IVB dichalcogenide monolayers. *J. Mater. Chem. A* **2018**, *6*, 24885−24898.

(28) Rawat, A.; Mohanta, M. K.; Jena, N.; Dimple; Ahammed, R.; De Sarkar, A. Nanoscale Interfaces of Janus Monolayers of Transition Metal Dichalcogenides for 2D Photovoltaic and Piezoelectric Applications. *J. Phys. Chem. C* **2020**, *124*, 10385−10397.

(29) Nguyen, H. T. T.; Tuan, V. V.; Nguyen, C. V.; Phuc, H. V.; Tong, H. D.; Nguyen, S.-T.; Hieu, N. N. Electronic and optical properties of a Janus SnSSe monolayer: effects of strain and electric field. *Phys. Chem. Chem. Phys.* **2020**, *22*, 11637−11643.

(30) Guo, S.-D.; Guo, X.-S.; Han, R.-Y.; Deng, Y. Predicted Janus SnSSe monolayer: a comprehensive first-principles study. *Phys. Chem. Chem. Phys.* **2019**, *21*, 24620−24628.

(31) Kahraman, Z.; Kandemir, A.; Yagmurcukardes, M.; Sahin, H. Single-Layer Janus-Type Platinum Dichalcogenides and Their Heterostructures. *J. Phys. Chem. C* **2019**, *123*, 4549−4557.

(32) Sino, P. A. L.; Feng, L.-Y.; Villaos, R. A. B.; Cruzado, H. N.; Huang, Z.-Q.; Hsu, C.-H.; Chuang, F.-C. Anisotropic Rashba splitting in Pt-based Janus monolayers PtXY (X,Y = S, Se, or Te). *Nanoscale Adv.* **2021**, *3*, 6608−6616.

(33) Vo, D. D.; Vu, T. V.; Al-Qaisi, S.; Tong, H. D.; Le, T. S.; Nguyen, C. V.; Phuc, H. V.; Luong, H. L.; Jappor, H. R.; Obeid, M. M.; Hieu, N. N. Janus monolayer PtSSe under external electric field and strain: A first principles study on electronic structure and optical properties. *Superlattices Microstruct.* **2020**, *147*, 106683.

(34) Cui, H.; Yang, T.; Peng, X.; Zhang, G. First-principles screening upon Janus PtXY (X, Y = S, Se and Te) monolayer under applied biaxial strains and electric fields. *J. Mater. Res. Technol.* **2022**, *18*, 1218−1229.

(35) Kresse, G.; Furthmüller, J. Efficient iterative schemes forab initiototal-energy calculations using a plane-wave basis set. *Phys. Rev. B: Condens. Matter Mater. Phys.* **1996**, *54*, 11169−11186.
(36) Kresse, G.; Furthmüller, J. Efficiency of ab-initio total energy calculations for metals and semiconductors using a plane-wave basis set. *Comput. Mater. Sci.* **1996**, *6*, 15−50.
(37) Blöchl, P. E. Projector augmented-wave method. *Phys. Rev. B: Condens. Matter Mater. Phys.* **1994**, *50*, 17953−17979.
(38) Perdew, J. P.; Burke, K.; Ernzerhof, M. Generalized Gradient Approximation Made Simple. *Phys. Rev. Lett.* **1996**, *77*, 3865−3868.
(39) Togo, A.; Tanaka, I. First principles phonon calculations in materials science. *Scr. Mater.* **2015**, *108*, 1−5.
(40) Krukau, A. V.; Vydrov, O. A.; Izmaylov, A. F.; Scuseria, G. E. Influence of the exchange screening parameter on the performance of screened hybrid functionals. *J. Chem. Phys.* **2006**, *125*, 224106.
(41) Henkelman, G.; Arnaldsson, A.; Jónsson, H. A fast and robust algorithm for Bader decomposition of charge density. *Comput. Mater. Sci.* **2006**, *36*, 354−360.
(42) Cadelano, E.; Palla, P. L.; Giordano, S.; Colombo, L. Elastic properties of hydrogenated graphene. *Phys. Rev. B: Condens. Matter Mater. Phys.* **2010**, *82*, 235414.
(43) Miró, P.; Ghorbani-Asl, M.; Heine, T. Two Dimensional Materials Beyond MoS_2: Noble-Transition-Metal Dichalcogenides. *Angew. Chem., Int. Ed.* **2014**, *53*, 3015−3018.
(44) Zhao, Y.; Qiao, J.; Yu, Z.; Yu, P.; Xu, K.; Lau, S. P.; Zhou, W.; Liu, Z.; Wang, X.; Ji, W.; Chai, Y. High-Electron-Mobility and Air-Stable 2D Layered $PtSe_2$ FETs. *Adv. Mater.* **2017**, *29*, 1604230.
(45) Mouhat, F.; Coudert, F.-X. Necessary and sufficient elastic stability conditions in various crystal systems. *Phys. Rev. B: Condens. Matter Mater. Phys.* **2014**, *90*, 224104.
(46) Lee, C.; Wei, X.; Kysar, J. W.; Hone, J. Measurement of the Elastic Properties and Intrinsic Strength of Monolayer Graphene. *Science* **2008**, *321*, 385−388.
(47) Zhu, H.; Wang, Y.; Xiao, J.; Liu, M.; Xiong, S.; Wong, Z. J.; Ye, Z.; Ye, Y.; Yin, X.; Zhang, X. Observation of piezoelectricity in free-standing monolayer MoS_2. *Nat. Nanotechnol.* **2015**, *10*, 151−155.
(48) Li, M.; Dai, J.; Zeng, X. C. Tuning the electronic properties of transition-metal trichalcogenides via tensile strain. *Nanoscale* **2015**, *7*, 15385−15391.
(49) Zhou, Y.; Wang, Z.; Yang, P.; Zu, X.; Yang, L.; Sun, X.; Gao, F. Tensile Strain Switched Ferromagnetism in Layered NbS_2 and $NbSe_2$. *ACS Nano* **2012**, *6*, 9727−9736.
(50) Bhattacharyya, S.; Singh, A. K. Semiconductor-metal transition in semiconducting bilayer sheets of transition-metal dichalcogenides. *Phys. Rev. B: Condens. Matter Mater. Phys.* **2012**, *86*, 075454.
(51) Yun, W. S.; Han, S. W.; Hong, S. C.; Kim, I. G.; Lee, J. D. Thickness and strain effects on electronic structures of transition metal dichalcogenides: 2H-MX_2 semiconductors (M = Mo, W; X = S, Se, Te). *Phys. Rev. B: Condens. Matter Mater. Phys.* **2012**, *85*, 033305.
(52) Conley, H. J.; Wang, B.; Ziegler, J. I.; Haglund, R. F., Jr.; Pantelides, S. T.; Bolotin, K. I. Bandgap Engineering of Strained Monolayer and Bilayer MoS_2. *Nano Lett.* **2013**, *13*, 3626−3630.

https://doi.org/10.1021/acsomega.2c07271
ACS Omega 2023, 8, 5715−5721